Effect of Thermal Treatment on Cation Local Structure in Manganese-Neutralized Sulfonated Polystyrene Ionomers

Richard A. Register,† Ashish Sen,‡,§ Robert A. Weiss,‡ and Stuart L. Cooper*,†

Department of Chemical Engineering, University of Wisconsin, Madison, Wisconsin 53706, and Institute of Materials Science and Department of Chemical Engineering, University of Connecticut, Storrs, Connecticut 06268. *Received July 25, 1988; Revised Manuscript Received September 23, 1988*

ABSTRACT: Two sets of manganese-neutralized sulfonated polystyrenes, at 2.6 and 7.6 mol % sulfonation, were subjected to three sample treatments: solvent casting from tetrahydrofuran/water, solvent casting followed by annealing, and compression molding. Both as-cast samples were void of ionic aggregates, as evidenced by the absence of a peak in their small-angle X-ray scattering (SAXS) patterns. Upon annealing, the SAXS peak appeared, indicating the formation of ionic aggregates. The compression-molded 7.6 mol % material also exhibited the SAXS peak, while the compression-molded 2.6 mol % material did not, possibly due to a slower rate of aggregation in the lower ion content material. The local coordination structure about the Mn^{2+} cation was examined by extended X-ray absorption fine structure (EXAFS) spectroscopy and found to be nearly identical for all six samples despite the differences in the state of aggregation. That the local structure is unaffected by the microdomain structure reflects the difference in size scale probed by SAXS and EXAFS.

I. Introduction

When a nonionic monomer is copolymerized with a small amount of ionic comonomer, profound changes in properties are observed relative to the nonionic parent polymer. The ionic copolymers, termed ionomers, typically contain less than 10 mol % of a sulfonic or carboxylic acid-bearing monomer and are neutralized with metal cations. The marked increases in, for example, modulus and tear and abrasion resistance and the dramatic alterations in ion-transport properties[1-3] that occur in these materials are now accepted as being due to aggregation of the ionic groups[4,5] into microdomains.

Because of the small size of these ionic aggregates, diffraction techniques can reveal little regarding their internal structure. On the other hand, extended X-ray absorption fine structure (EXAFS) spectroscopy is a powerful technique for determining the local atomic environment about a specific atom and has been profitably applied to numerous ionomers.[6-17] The EXAFS signal is a modulation of the X-ray absorption coefficient on the high-energy side of an element's absorption edge, and it contains information on the coordination shells surrounding that atom. The type and number of atoms in a shell, as well as the distance to and disorder within a shell, are reflected in the EXAFS data. As such, EXAFS can probe the environment around ions that reside in ionic aggregates, as well as dispersed ionic groups and even ions in solution.[10]

One ionomer that has been studied in detail by numerous investigators[6,8,11,13,18-26] is sulfonated polystyrene (SPS), produced by a postpolymerization sulfonation of polystyrene to place sulfonic acid groups at the para positions of the phenyl rings.[25] The distribution of ionic sites along the polymer backbone is random. SPS generally exhibits the usual microphase-separated ionomer morphology, as evidenced by the presence of a peak in the small-angle X-ray scattering (SAXS) pattern[18,19,21,22] at a momentum transfer vector magnitude q ($q = (4\pi/\lambda) \sin \theta$, where 2θ is the scattering angle and λ the wavelength of the radiation) of approximately 1.5 nm^{-1}, corresponding to a Bragg spacing of 4 nm. Recently, however, it was found[23] that a sample of SPS (7.6 mol % sulfonation) neutralized with Mn^{2+} and cast from a tetrahydrofuran/water (90/10, v/v) solution failed to exhibit the ionomer SAXS peak, although other casting solvents produced an ionomer peak of varying intensity. When the sample was heated[26] to 165 °C, the SAXS peak became visible at 1.7 nm^{-1}. The glass transition in the as-cast material occurred at 100 °C, as determined by differential scanning calorimetry. The central conclusion from these experiments was that, in the as-cast state, the material is free of ionic aggregates, which develop upon heating as the ionic groups gain sufficient mobility in the polystyrene matrix to coalesce.

The experiments discussed above show that the cation environment on a microphase scale can be altered in these materials through the choice of casting solvent, thermal history, or both. A related question is how the local environment, on the scale of atomic distances, is affected by this process. For this purpose, we have employed EXAFS to study the local cation environment in two MnSPS samples (2.6 and 7.6 mol % sulfonation) subjected to three thermal histories (solvent casting from THF/water, solvent casting followed by annealing at 120 °C, and compression molding at 188 °C). The state of aggregation of the ionic groups was determined by the presence or absence of the ionomer peak in the SAXS pattern.

II. Experimental Section

A. Sample Preparation. The acid form of SPS was prepared by sulfonation in solution with acetyl sulfate, as described previously.[25] The acid SPS was converted to the manganese ionomer by neutralizing with the stoichiometric amount of an aqueous solution of manganese acetate tetrahydrate. The ionomer was then recovered by precipitation into deionized water and drying under vacuum at 80 °C for 48 h. The sulfonation level was determined by elemental analysis for sulfur.

To prepare the as-cast sample, a 10% (w/w) solution of the ionomer in 90/10 (v/v) tetrahydrofuran/water was prepared and cast onto a glass plate. The solvent was evaporated in air and then under vacuum at 60 °C for 5 days. The films so prepared were approximately 50–200 μm thick. The annealed samples were prepared by heating a portion of the as-cast films at 120 °C under vacuum for 4 days. The compression-molded samples were prepared by heating the ionomers to 188 °C at 11 MPa and allowing them to cool to room temperature over a period of 2 h. The 2.6 mol % materials were translucent yellow while the 7.6 mol % materials were opaque brown. The materials were stored in a desiccator over $CaSO_4$. In the discussion that follows, the

* To whom correspondence should be addressed.
† University of Wisconsin.
‡ University of Connecticut.
§ Present address: Texaco Research Center, P.O. Box 509, Beacon, NY 12508.

0024-9297/89/2222-2224$01.50/0

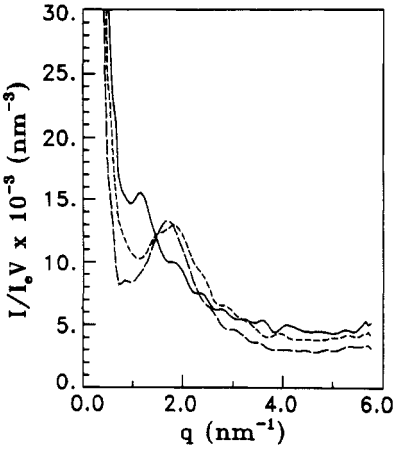

Figure 1. SAXS patterns for the 7.6 mol % series: (—) S76, (---) A76, (--) C76.

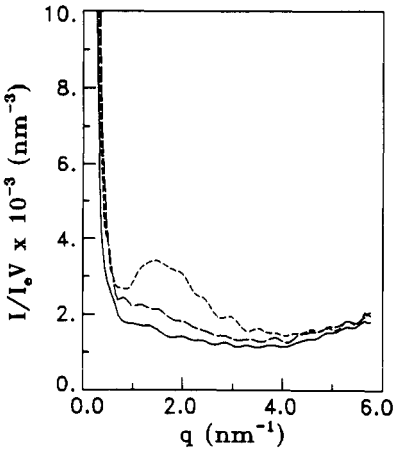

Figure 2. SAXS patterns for the 2.6 mol % series: (—) S26, (---) A26, (--) C26.

samples will be identified by a three-symbol code; the first symbol refers to the thermal treatment ("S" for as-cast from solvent, "A" for solvent-cast and then annealed, "C" for compression molded), and the last two characters are the sulfonation level in tenths of a mole percent (i.e., "S76" is the as-cast 7.6 mol % sulfonation sample).

B. SAXS Measurements. The samples for the small-angle X-ray scattering (SAXS) experiments were stacked films contained between polyimide windows to provide support. The SAXS instrumentation used has been described previously.[14] The X-ray generator was operated at 30-kV accelerating potential and 15-mA emission current, and the Cu Kα X-rays were collimated into a line measuring 0.75 cm by 100 μm at the sample. The data were corrected for detector sensitivity, empty beam and window scattering, and sample transmittance. A moderate amount of cubic spline smoothing was applied to the data, which were then desmeared by the iterative method of Lake[27] and placed on an absolute intensity scale by comparison with a calibrated Lupolen polyethylene standard.[28] However, the as-cast and annealed specimens were of nonuniform thickness and were somewhat warped as well, which made thickness measurements difficult. In practice, the effective thickness was calculated by measuring the thickness and transmittance of the compression-molded samples, computing the linear attenuation coefficient, and then calculating the thickness of the as-cast and annealed specimens from their measured transmittances, using the linear attenuation coefficient for the compression-molded sample of the same elemental composition. The nonuniform thickness of the samples also introduces error into the desmearing process. However, treating the data in this manner does allow for some comparison between the different samples. More importantly, all that is really necessary for this investigation is to confirm the presence or absence of the ionic peak.

C. EXAFS Measurements. The transmission EXAFS spectra were collected in the vicinity of the manganese K-edge (6539.0 eV) on the C-1 station of the Cornell High Energy Synchrotron Source (CHESS). The same specimens were used for both SAXS and EXAFS experiments, including the polyimide windows. Data reduction followed a standard procedure of preedge and postedge background removal, extraction of the EXAFS oscillations $\chi(k)$, Fourier transformation of $\chi(k)$, and finally application of an inverse transform to isolate the EXAFS contribution from a selected region in real space.[29-31] The model compounds chosen for this study were MnO (Alfa, 99.5%) and $Mn(CH_3COO_2)_2 \cdot 4H_2O$ (MCB, reagent). The model compound samples were prepared by spreading layers of the powdered material on pieces of polyimide tape and stacking the pieces to obtain a reasonably homogeneous absorbance across the film.

III. Results and Analysis

A. SAXS Results. The SAXS results for the 7.6 mol % samples are shown in Figure 1. These figures strongly resemble those obtained earlier by heating a sample similar to S76 and simultaneously observing the SAXS pattern.[26] The ripples present in the S76 SAXS pattern arise from residual (unsmoothed) statistical counting noise, which is most severe for the extremely thin S76 sample. S76 exhibits no clear ionomer peak, although a shoulder is visible on the low-q upturn. In previous synchrotron SAXS studies on a similar material, this shoulder was found to disappear upon heating to 100 °C, without moving to the higher q values characteristic of the annealed or compression-molded samples.[40] Since the as-cast samples were vacuum-dried at 60 °C, while the specimen's glass transition is approximately 100 °C, this suggests that the shoulder may be associated with residual solvent. In any case, comparison of the three curves in Figure 1 shows that S76 does not exhibit the "usual" ionomer peak.

The annealed sample (A76) exhibits a clear ionomer peak near 1.7 nm^{-1}, which is even more pronounced in the compression-molded sample. Note that the three curves in Figure 1 should approximately superimpose at high q, since the magnitude of thermal fluctuations and wide-angle scattering from the polystyrene backbone should be nearly identical for all three samples. The fact that the curves do not superimpose exactly reflects the difficulties posed by using warped specimens of nonuniform thickness, as discussed in the Experimental Section. It should also be noted that the strength of the upturn at very small angles decreases as the peak intensity increases, as was found previously[26] upon heating a sample similar to S76. This suggests that an interconversion of ions between two environments, such as "dispersed" and "aggregated"[32] or "multiplets" and "clusters",[5] is occurring.

The SAXS patterns for the 2.6 mol % samples, shown in Figure 2, do not quite parallel those for the 7.6 mol % samples. The S26 and A26 samples do clearly represent unaggregated and aggregated systems, with sample C26 falling somewhere in between. In particular, the compression-molded sample does not exhibit a sizable ionomer peak, while the annealed sample does. Since the maximum temperature achieved in compression molding exceeds that used in annealing, the absence of an ionomer peak in C26 suggests that the shorter time allowed for compression molding was insufficient to allow the formation of ionic aggregates. Further, the fact that sample C76 exhibits a clear peak, while C26 does not, suggests that a higher ion content allows the aggregation process to occur more rapidly. Since the distance an ionic group must diffuse to incorporate itself into an aggregate increases with decreasing ion content, this suggestion is qualitatively reasonable.

Previous simultaneous SAXS–DSC studies[26] have concentrated on the development of the ionomer peak during annealing for samples similar to S76, and specimens of S26

Table I
EXAFS Structural Parameters

sample	shell no. (j)	shell element	ΔE_0, eV	R_j, Å	$N_j\gamma_j$	N_j	σ_j, Å	Q,[a] %
MnO	1	O	18.5	2.21	2.31	5.2	0.071	4.5
	2	Mn	6.1	3.12	6.48		0.092	5.6
$MnAc_2$	1	O	18.6	2.17	2.94	6.6	0.076	5.6
S76	1	O	21.5	2.18	2.08	4.7	0.066	6.8
A76	1	O	21.0	2.16	2.13	4.7	0.073	6.7
C76	1	O	21.2	2.16	2.36	5.3	0.080	5.8
S26	1	O	19.3	2.17	2.60	5.8	0.061	6.8
A26	1	O	14.0	2.10	2.44	5.3	0.057	2.3
C26	1	O	16.6	2.14	3.80	8.4	0.098	2.5

[a] The quality of fit, Q, is defined as the square root of the ratio of the sum of the squares of the residue to the sum of the squares of the data.

will be investigated by this technique in the future. The brief SAXS results presented here are intended only to serve as a qualitative indication of the state of aggregation in these materials, which will form the basis for interpreting the EXAFS results in the following section.

B. EXAFS Results. The manganese oxide (MnO) and manganese diacetate tetrahydrate (abbreviated $MnAc_2$) model compounds have only oxygen atoms in the first coordination shell, as was expected for the MnSPS samples. Additionally, the MnO sample has a strong second coordination shell composed of Mn atoms, which would be necessary for analysis of the EXAFS data if such Mn–Mn distances were observed in the ionomers.

Because their crystallographic structures are well-established, it is useful to examine the EXAFS from these model compounds in some detail to compare with the relatively disordered environment typically found in ionomers. The absorption modulation, which is the EXAFS signal, arises because photoelectrons, which are ejected by the absorbed X-rays, can be backscattered by atoms coordinated to the absorbing atom; superposition of the outgoing and backscattered electron waves gives rise to an interference pattern. The EXAFS signal $\chi(k)$, where k is the photoelectron wave vector, contains information on the number N_j and type of atoms in coordination shell j, the distance R_j to this shell, and the static and vibrational disorder of the shell, measured as the Debye–Waller factor σ_j. To convert the EXAFS signal from wave vector to real space, it is Fourier transformed, and the magnitude of the transform is termed the radial structure function, or RSF. Each nonartifactual peak in the RSF represents a distinct coordination shell; the peak positions are shifted slightly from the true shell distances by a phase shift ϕ_j that the photoelectron experiences in backscattering.

The EXAFS data were analyzed with single-electron single-scattering theory[30]

$$\chi(k) = \sum_j \frac{N_j\gamma_j}{kR_j^2} f_j(k) \sin [2kR_j + \phi_j(k)] \exp(-2k_j^2\sigma_j^2) \quad (1)$$

where k is the wave vector defined as $k = (2\pi/h)[2m(E - E_0)]^{1/2}$, E is the incident X-ray energy, h is Planck's constant, and m is the mass of an electron. E_0 is approximately equal to the edge energy but is allowed to vary slightly to provide the best fit to the data,[33] correcting for any errors in energy calibration or differences in chemical environment relative to the calibrant (Mn foil). The shift is given below by the parameter ΔE_0, where $E_0 = E_e - \Delta E_0$, and E_e is the experimental edge energy. γ_j accounts for the amplitude reduction due to inelastic scattering and is approximated as $\exp(-2R_j/\lambda)$, with λ defining a mean-free-path parameter. λ is obtained from the EXAFS data and known crystal structures for the model compounds. $f_j(k)$ and $\phi_j(k)$ are the backscattering amplitude and phase-shift functions, respectively, which are characteristic of the types of atoms in shell j and the absorbing atom. The calculations of Teo and Lee[33] were used throughout for these functions, except for slight modifications to accommodate experimental data from model compounds studied previously.[41] The accuracies of the R_j and N_j determinations are often quoted[34,35] as 1% and 20%, respectively, although the accuracies depend strongly on the quality of the data, both in signal-to-noise ratio and the breadth of the usable wave-vector range.

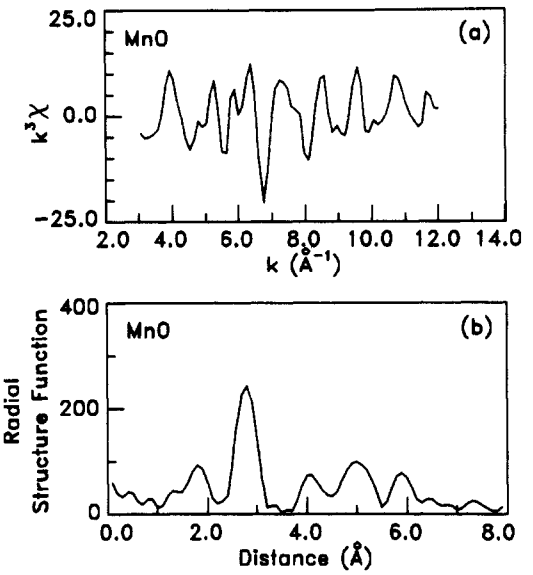

Figure 3. EXAFS data for MnO: (a) $k^3\chi$ vs k, (b) radial structure function.

The EXAFS data for MnO are shown in Figure 3. The RSF (Figure 3b) shows several nonartifactual peaks; those that appear at distances less than 1.5 Å are artifacts of imperfect background substraction. The first shell, at about 1.8 Å in the RSF, arises from six oxygen atoms at a distance of 2.22 Å as determined crystallographically.[36] The difference in these distance values is due to the phase shift discussed above. The second, and much larger, peak at 2.8 Å arises from 12 Mn atoms at a distance of 3.14 Å. The parameters obtained from the fit to the back-transform of each peak are listed in Table I and are in good agreement with the crystallographic distances. The mean free path λ for the first shell is found to be 4.6 Å, using the true value $N_1 = 6$.

The same plots for $MnAc_2$ are shown in Figure 4. The crystallographic data[37] indicate that the first shell actually comprises several types of oxygen atoms and that the average Mn–O distance is 2.19 ± 0.04 Å. The differences between the Mn–O distances are too small to be discerned by EXAFS, which should perceive the first shell as being made up of six oxygen atoms at 2.19 Å. The results of the

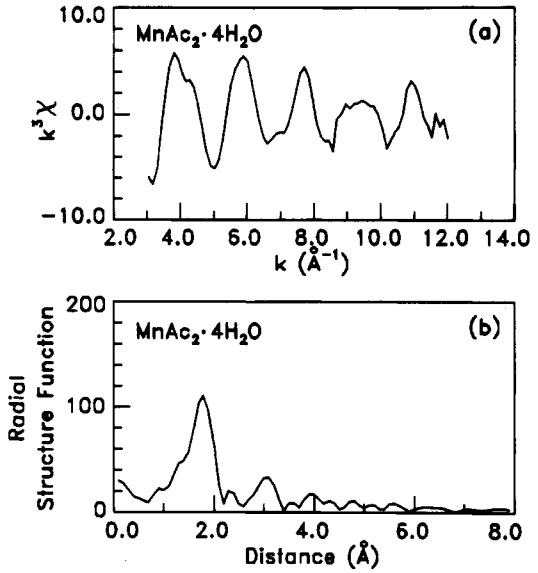

Figure 4. EXAFS data for $MnAc_2$: (a) $k^3\chi$ vs k, (b) radial structure function.

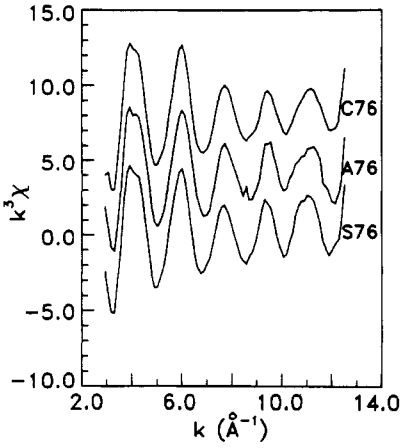

Figure 5. EXAFS data for the 7.6 mol % MnSPS, $k^3\chi$ vs k. The curve for A76 has been shifted upward 4 units, while C76 has been shifted upward 8 units, for clarity.

fit to the back-transform of the second peak are shown in Table I and are in good agreement with the crystallographic structure. The value of λ computed from this data set is 6.1 Å; an average value of 5.4 Å, from the MnO and $MnAc_2$ data, was used to analyze the ionomer EXAFS. The second peak in the $MnAc_2$ RSF is considerably more complicated, with contributions arising from Mn–O, Mn–C, and Mn–Mn distances based on the crystal structure. No attempt was made to analyze this peak.

The EXAFS data for the 7.6 mol % MnSPS are shown in Figures 5 and 6. As can be seen in Figure 5, the $k^3\chi$ vs k data sets appear virtually indistinguishable for the three thermal treatments. This similarity is carried over directly into the RSFs, as shown in Figure 6. Only one shell is visible in each RSF; this corresponds to the presence of a single period in the $k^3\chi$ vs k data for the ionomers, in contrast to that for the model compounds.

An example of the fitting process is shown in Figure 7. In Figure 7a, the circles represent the back-transform of the first peak in the RSF, or "filtered" $k^3\chi$ data, while the solid line represents the fit. In Figure 7b, the RSF obtained by transforming the $k^3\chi$ data is shown as the dashed line, while the solid line is the transform of the filtered $k^3\chi$ data. The fits are good in both cases. Note that, in some data sets, a small shoulder is visible on the low-distance side of the first peak in the RSF. This peak is at too short

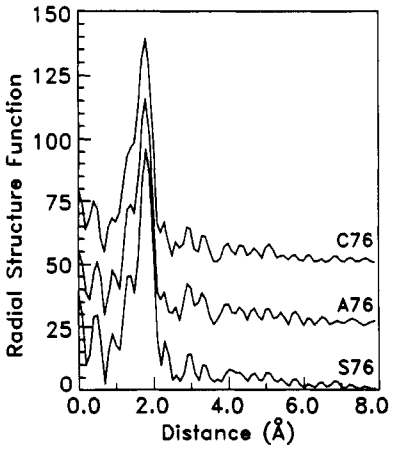

Figure 6. EXAFS data for the 7.6 mol % MnSPS, RSF. The curve for A76 has been shifted upward 25 units, while C76 has been shifted upward 50 units, for clarity.

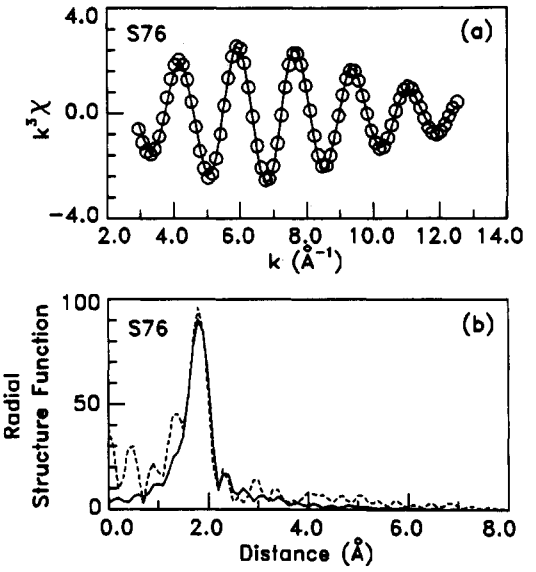

Figure 7. Example of EXAFS model fitting, for sample S76: (a) Circles are the back-transform of the first peak in the RSF; solid line is the fit. (b) Dashed line is the RSF; solid line is the fit.

a distance to arise from a real shell, although such a feature is commonly observed,[7-9,12,16,17] and can be seen in the data for the model compounds as well. As mentioned previously, this artifact arises from incomplete background subtraction and could interfere slightly with the data analysis if it makes a significant contribution to the first shell peak.

The structural parameters obtained from the analysis are listed in Table I. The values of N_1 lie in the range 4.7–5.3; these numbers are within 25% of the value of N_1 found for the two model compounds, so the Mn^{2+} ions are most likely 6-fold-coordinated. Note that using a value of 5.4 Å for λ gives N_1 equal to 5.2 for MnO and 6.6 for $MnAc_2$, whereas both are known to be 6 from their crystal structures. This gives a measure of the accuracy of EXAFS in determining N_j. The Mn–O distance is comparable to that found in the model compounds as well. The three thermal treatments appear to have the same effect on the local structure, with none of them producing a second shell.

The EXAFS data for the 2.6 mol % samples are shown in Figures 8 and 9. Because of the lower ion contents in these materials, the signal-to-noise ratio and the usable wave-vector range are reduced when compared with the 7.6 mol % samples. In Figure 9, the first shell peak increases in breadth in the order S26 < C26 < A26, the

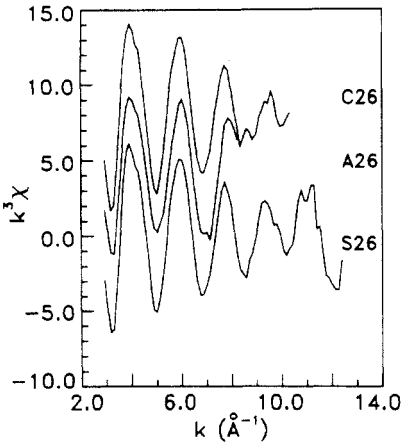

Figure 8. EXAFS data for the 2.6 mol % MnSPS, $k^3\chi$ vs k. The curve for A26 has been shifted upward 4 units, while C26 has been shifted upward 8 units, for clarity.

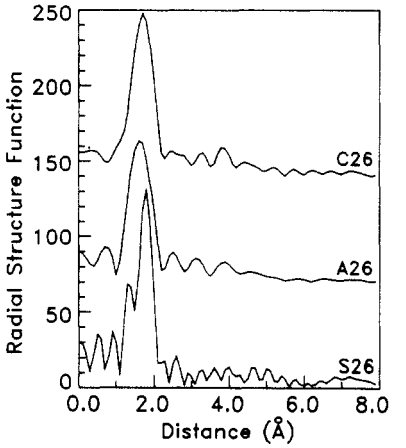

Figure 9. EXAFS data for the 2.6 mol % MnSPS, RSF. The curve for A26 has been shifted upward 70 units, while C26 has been shifted upward 140 units, for clarity.

opposite of the trend in breadth of wave-vector range. When differences in signal-to-noise ratio and wave-vector range are accounted for, the $k^3\chi$ and RSF data are essentially identical for all three thermal treatments. Moreover, the data are very similar to those for the 7.6 mol % samples. The parameters listed in Table I confirm this conclusion. The slight reduction of the Mn–O distance observed for the A26 and C26 samples compared with the S26 sample is tied to the diminution of the unsable wave-vector range, which provides fewer periods of $k^3\chi$ to model, and to a possible contribution from the low-distance shoulder discussed above, which has merged with the peak in the A26 and C26 samples. This small change should not be interpreted as significant. The N_1 value for C26 is found to be anomalously large (8.4), which is related to the large value of σ_1 also found for C26, since these two parameters are positively correlated in the regression of eq 1. The similarity of the $k^3\chi$ data and RSFs, however, indicates that this material has the same structure as S26 and A26, that is, 6-fold coordination by oxygen.

IV. Discussion

The EXAFS results indicate that the local structure about the Mn^{2+} cation in these materials is unaltered by ionic aggregation. While this appears at first to be a surprising result, the key to interpretation lies in the difference in the size scale probed by EXAFS and SAXS. It is entirely possible to have an ionic aggregate whose internal structure is highly disordered. For example, EXAFS data for a cesium-neutralized polyurethane ionomer[38] fail to exhibit even a single clear peak in the RSF, while SAXS experiments clearly show the "ionomer" peak. A study of carboxy-telechelic polyisoprene ionomers[14] showed that wide differences in local structure could be found with differing cations and moisture contents, as evidenced by the size of a metal–metal peak in the RSF; however, the SAXS patterns from these materials were qualitatively similar. These results show that, even when the ionic groups are aggregated, the aggregates may be too disordered internally to exhibit the well-defined metal–metal distance necessary to give a second peak in the RSF.

One question not addressed thus far is why no second shell is visible in the EXAFS RSF from the sulfur atoms in the sulfonate group. If the oxygens in the first shell are sulfonate oxygens, this should lead to a well-defined Mn–S distance, which should appear as a second shell. Indeed, previous studies[8,11] of a zinc-neutralized SPS did exhibit a second shell, which was well-described by a combination of sulfur and oxygen atoms, as would be expected from a bidentate sulfonate group. However, to obtain a material with this structure, the sample had to be dried at 120 °C under vacuum for 24 h to remove residual water. It was also found[8] that strontium-neutralized SPS subjected to the same thermal treatment did not exhibit a second coordination shell. While Mn (group VIIA) might be expected to resemble Zn (group IIB) more than Sr (group IIA) in its behavior, it may be that the results found for Zn represent a special case. A recent EXAFS study[13] has shown that small amounts of water destroy the second-shell peak in ZnSPS by displacing some or all of the sulfonate oxygens, leading to an EXAFS RSF that resembles that for SrSPS or that observed here for MnSPS. This suggests that the thermal treatments used here could not remove the last traces of bound water from MnSPS, though the same annealing treatment is sufficient to thoroughly dry ZnSPS. While a trace amount of water is unlikely to affect the aggregation of the ionic groups into microdomains, it can profoundly affect the local structure. Vlaic et al.[39] have used EXAFS to demonstrate the strong effect that sample preparation conditions can have on the cation local structure in ionomers.

Interestingly, X-band electron spin resonance (ESR) measurements on samples similar to S76 and A76 show a single broad line in both cases.[26] A single broad line is characteristic of Mn–Mn interactions on a size scale smaller than 8 Å (between the scales probed by SAXS and EXAFS). At lower ion contents, below about 5 mol %, isolated Mn^{2+} ions are also present, which exhibit a characteristic six-line hyperfine pattern.[42] This indicates that, in S76, the ionic groups do not exist individually but form couples or small multiplets. These structures can be condensed into larger aggregates by heating at elevated temperature for sufficient time, as shown by the presence of the SAXS peak in A76 and C76.

V. Conclusions

Two sets of MnSPS, at 2.6 and 7.6 mol % sulfonation, subjected to three thermal treatments (as-cast from solvent, annealed, and compression molded) were examined by EXAFS. These samples did not exhibit the ionomer SAXS peak in the as-cast state, but upon annealing (both sets) or compression molding (7.6 mol % only), the SAXS peak developed, indicating the formation of ionic aggregates. The absence of the SAXS peak in the compression-molded 2.6 mol % sample may reflect a slower rate of aggregation at the lower ion content. The local structure about the Mn^{2+} cation was found to be similar for all samples and resembled that in the first shell of the model compounds manganese oxide and manganese acetate tet-

rahydrate: 6-fold coordination by oxygen. No second shell was observable for these ionomers, in contrast to the model compounds. The absence of a discernable second shell due to sulfonate sulfur is ascribed to the presence of trace amounts of water, which displace some or all of the sulfonate oxygens in the first coordination shell. The lack of any change in the local structure upon aggregation is explained on the basis of the different length scales probed by SAXS and EXAFS; the aggregates are found to be too disordered internally to exhibit a well-defined Mn–Mn distance.

Acknowledgment. R.A.R. thanks the staff of the Cornell High Energy Synchrotron Source (CHESS) of the Wilson Synchrotron Laboratory at Cornell University for the opportunity to carry out the EXAFS experiments and the Fannie and John Hertz Foundation for financial support while this work was conducted. The assistance of Patrick A. Thompson in collecting the EXAFS data is gratefully acknowledged. Partial support of this research was provided by the Polymers Section of the Division of Materials Research of the National Science Foundation through Grants DMR-86-03839 (S.L.C.) and DMR-84-07098 (R.A.W.) and by the Petroleum Research Fund, administered by the American Chemical Society, through Grant 19205-AC7 (R.A.W.).

Registry No. MnO, 1344-43-0; $Mn(CH_3COO_2)_2$, 638-38-0.

References and Notes

(1) Eisenberg, A., King, M., Eds. *Ion Containing Polymers*; Halsted-Wiley: New York, 1975.
(2) Bazuin, C. G.; Eisenberg, A. *Ind. Eng. Chem. Prod. Res. Dev.* **1981**, *20*, 271.
(3) MacKnight, W. J.; Earnest, T. R. *Macromol. Rev.* **1981**, *16*, 41.
(4) Wilson, F. C.; Longworth, R.; Vaughan, D. J. *Polym. Prepr. (Am. Chem. Soc., Div. Polym. Chem.)* **1968**, *9*, 505.
(5) Eisenberg, A. *Macromolecules* **1970**, *3*, 147.
(6) Yarusso, D. J.; Cooper, S. L.; Knapp, G. S.; Georgopoulos, P. *J. Polym. Sci., Polym. Lett. Ed.* **1980**, *18*, 557.
(7) Pan, H. K.; Yarusso, D. J.; Knapp, G. S.; Cooper, S. L. *J. Polym. Sci., Polym. Phys. Ed.* **1983**, *21*, 1389.
(8) Yarusso, D. J.; Ding, Y. S.; Pan, H. K.; Cooper, S. L. *J. Polym. Sci., Polym. Phys. Ed.* **1984**, *22*, 2073.
(9) Pan, H. K.; Yarusso, D. J.; Knapp, G. S.; Pinéri, M.; Meagher, A.; Coey, J. M. D.; Cooper, S. L. *J. Chem. Phys.* **1983**, *79*, 4736.
(10) Pan, H. K.; Knapp, G. S.; Cooper, S. L. *Colloid Polym. Sci.* **1984**, *262*, 734.
(11) Ding, Y. S.; Yarusso, D. J.; Pan, H. K.; Cooper, S. L. *J. Appl. Phys.* **1984**, *56*, 2396.
(12) Pan, H. K.; Meagher, A.; Pinéri, M.; Knapp, G. S.; Cooper, S. L. *J. Chem. Phys.* **1985**, *82*, 1529.
(13) Ding, Y. S.; Register, R. A.; Nagarjan, M. R.; Pan, H. K.; Cooper, S. L. *J. Polym. Sci., Polym. Phys. Ed.* **1988**, *26*, 289.
(14) Register, R. A.; Foucart, M.; Jérôme, R.; Ding, Y. S.; Cooper, S. L. *Macromolecules* **1988**, *21*, 1009; correction, **1988**, *21*, 2652.
(15) Jérôme, R.; Vlaic, G.; Williams, C. E. *J. Phys. Lett.* **1983**, *44*, L-717.
(16) Galland, D.; Belakhovsky, M.; Medrignac, F.; Pinéri, M.; Vlaic, G.; Jérôme, R. *Polymer* **1986**, *27*, 883.
(17) Meagher, A.; Coey, J. M. D.; Belakhovsky, M.; Pinéri, M.; Jérôme, R.; Vlaic, G.; Williams, C.; Dang, N. V. *Polymer* **1986**, *27*, 979.
(18) Yarusso, D. J.; Cooper, S. L. *Macromolecules* **1983**, *16*, 1871.
(19) Yarusso, D. J.; Cooper, S. L. *Polymer* **1985**, *26*, 371.
(20) Weiss, R. A. *J. Polym. Sci., Polym. Phys. Ed.* **1982**, *20*, 65.
(21) Weiss, R. A.; Lefelar, J.; Toriumi, H. *J. Polym. Sci., Polym. Lett. Ed.* **1983**, *21*, 661.
(22) Weiss, R. A.; Lefelar, J. *Polymer* **1986**, *27*, 3.
(23) Fitzgerald, J. J.; Kim, D.; Weiss, R. A. *J. Polym. Sci., Polym. Lett. Ed.* **1986**, *24*, 263.
(24) Earnest, T. R.; Higgins, J. S.; Handlin, D. L.; MacKnight, W. J. *Macromolecules* **1981**, *14*, 192.
(25) Makowski, H. S.; Lundberg, R. D.; Singhal, G. S. U.S. Patent 3,870,841, to Exxon Research and Engineering Co., March 11, 1975.
(26) Galambos, A. F.; Stockton, W. B.; Koberstein, J. T.; Sen, A.; Weiss, R. A.; Russell, T. P. *Macromolecules* **1987**, *20*, 3091.
(27) Lake, J. A. *Acta Crystallogr.* **1967**, *23*, 191.
(28) Pilz, I.; Kratky, O. *J. Colloid Interface Sci.* **1967**, *24*, 211.
(29) Sayers, D. E.; Stern, E. A.; Lytle, F. W. *Phys. Rev. Lett.* **1971**, *27*, 1024.
(30) Stern, E. A.; Sayers, D. E.; Lytle, F. W. *Phys. Rev. B* **1975**, *11*, 4836.
(31) Lee, P. A.; Citrin, P. H.; Eisenberger, P.; Kincaid, B. M. *Rev. Mod. Phys.* **1981**, *53*, 769.
(32) Ding, Y. S.; Hubbard, S. R.; Hodgson, K. O.; Register, R. A.; Cooper, S. L. *Macromolecules* **1988**, *21*, 1698.
(33) Teo, B. K.; Lee, P. A. *J. Am. Chem. Soc.* **1979**, *101*, 2815.
(34) Lengler, B.; Eisenberger, P. *Phys. Rev. B* **1980**, *22*, 4507.
(35) Stern, E. A.; Kim, K. *Phys. Rev. B* **1981**, *23*, 781.
(36) Donnay, J. D. H., Ondik, H. M., Eds. *Crystal Data: Determinative Tables*, 3rd ed., National Bureau of Standards: Washington, DC, 1973; Vol. II.
(37) Bertaut, E. F.; Duc, T. Q.; Burlet, P.; Burlet, P.; Thomas, M.; Moreau, J. M. *Acta Crystallogr.* **1974**, *B30*, 2234.
(38) Ding, Y. S. Ph.D. Thesis, University of Wisconsin—Madison, 1986.
(39) Vlaic, G.; Williams, C. E.; Jérôme, R.; Tant, M. R.; Wilkes, G. L. *Polymer* **1988**, *29*, 173.
(40) Galambos, A. F.; Stockton, W. B.; Koberstein, J. T.; Sen, A.; Weiss, R. A.; Russell, T. P., unpublished data.
(41) Pan, H. K. Ph.D. Thesis, University of Wisconsin—Madison, 1983.
(42) Toriumi, H.; Weiss, R. A.; Frank, H. A. *Macromolecules* **1984**, *17*, 2104.